Journal of Catalysis 260 (2008) 205–216

Contents lists available at ScienceDirect

Journal of Catalysis

www.elsevier.com/locate/jcat

Characterization of Fe/ZSM-5 DeNO$_x$ catalysts prepared by different methods: Relationships between active Fe sites and NH$_3$-SCR performance

Masaoki Iwasaki *, Kiyoshi Yamazaki, Koji Banno, Hirofumi Shinjoh

TOYOTA Central Research and Development Laboratories Inc., 41-1 Yokomichi, Nagakute-cho, Aichi 480-1192, Japan

ARTICLE INFO

Article history:
Received 11 June 2008
Revised 15 October 2008
Accepted 15 October 2008
Available online 28 October 2008

Keywords:
Nitric oxide
Reduction
Iron
ZSM-5
Ammonia
Temperature-programmed desorption
Ultraviolet and visible spectroscopy
Mössbauer spectroscopy
Fourier transform infrared spectroscopy
Active site

ABSTRACT

To identify and quantify active Fe species in the selective catalytic reduction (SCR) of NO by NH$_3$, a series of Fe/ZSM-5 catalysts was prepared by impregnation, reductive solid-state ion exchange, and chemical vapor deposition (CVD) under different levels of Fe loading, and was characterized by XRD, temperature-programmed desorption (TPD) of NH$_3$ and NO$_2$, and UV–vis, Mössbauer, and FT-IR spectroscopies. Their SCR activity depended strongly on the preparation method, and CVD was the most effective technique. Three types of Fe species were coexisted; aggregated α-Fe$_2$O$_3$ particles, Fe$_x$O$_y$ oligomer, and ion-exchanged oxo-Fe^{3+}. Relative concentration of oxo-Fe^{3+} as determined by T–O–T perturbation peak in FT-IR correlated with the higher temperature peak in NO$_2$-TPD, which was linearly related to the catalytic performance. Thus, oxo-Fe^{3+} sites were considered to be the active sites and were accurately quantified using NO$_2$-TPD. Furthermore, the turnover frequency was independent of the preparation method and Fe loading.

1. Introduction

Iron containing zeolites have attracted much interest due to their remarkable catalytic activity for selective catalytic reduction (SCR) of NO$_x$ (NO + NO$_2$) by NH$_3$ [1–6] or hydrocarbons [3,4,7–11], N$_2$O decomposition/reduction [12–15], oxidation of benzene to phenol [16], and selective oxidation of NH$_3$ to N$_2$ [17]. For reduction of NO$_x$ emission from mobile diesel engine, Fe/ZSM-5 is one of the most suitable catalysts because of its high activity and durability [1,2,8]. Although much effort has been invested in the characterization over Fe/ZSM-5, the active Fe sites for the SCR reaction are still under debate. The main reason for this continued uncertainty is the coexistence of many Fe species [3,4,7,9,18], isolated and/or binuclear Fe ions at ion exchange positions, small oligonuclear Fe$_x$O$_y$ clusters inside and/or outside the pores, and large Fe$_2$O$_3$ particles on the external surface, which prevent the identification of the active Fe sites. Furthermore, in many reactions only a small fraction of Fe sites actively participates in the catalytic cycle [5,9,19].

Joyner and Stockenhuber [7] have reported that Fe/ZSM-5 prepared by several methods contains isolated Fe cations and nanoclusters with an average composition of Fe$_4$O$_4$ using extended X-ray absorption fine structure spectroscopy (EXAFS). Correlations between catalytic activity and Fourier transform infrared (FT-IR) spectroscopy results for adsorbed NO indicated that the Fe$_4$O$_4$ nanoclusters were more active in the SCR by propene than the isolated cations. However, the relationship between catalytic activity and each species has been speculative, and the active Fe sites have not been quantified.

On the other hand, binuclear oxygen-bridged Fe sites, for which models are derived from EXAFS studies by several group [18,20,21], may be the active sites for SCR by hydrocarbons [8,10,11] and by NH$_3$ [22]. However, the correlation between the SCR activity and the active sites using several catalysts has not been investigated. In addition, EXAFS is unable to distinguish specific Fe species [9]. Thus, if samples contain a mixture of different Fe species, EXAFS is an unsuitable for analyzing active sites.

Schwidder et al. [4] have prepared a series of Fe/ZSM-5 catalysts using improved liquid ion exchange method containing 0.2–1.2 wt% Fe (Fe/Al: 0.033–0.195) and have investigated the nature of Fe sites using UV–vis, electron paramagnetic resonance (EPR), EXAFS, transmission electron microscopy (TEM), and SCR performance by isobutene and NH$_3$. By correlating the activities with the concentration of Fe sites as determined from UV–vis spectra, they have concluded that isolated Fe sites play major roles in both SCR reaction and that oligomers also contribute to the reactions; however, the oligomers are more active during unselective oxidation of the reductant. They have classified the UV–vis absorption into

* Corresponding author. Fax: +81 561 63 6712.
E-mail address: iwasaki@mosk.tytlabs.co.jp (M. Iwasaki).

0021-9517/$ – see front matter
doi:10.1016/j.jcat.2008.10.009

three categories (isolated Fe ions, oligometric clusters, and large particles) and have quantified each Fe species by deconvoluting the spectra [3,4]. However, this quantification must be regarded with caution because the extinction coefficient of each species is different and is not yet known. In addition, as their catalysts have been confined to one preparation method and low Fe content (Fe/Al < 0.2), the influence of other methods and of higher Fe content are not clear. If catalysts contain excess of Fe_2O_3 particles, the UV–vis spectra would become complicated and significantly difficult to analyze [23,24] because the absorption edge of these species depends on the particle size [25,26].

The distribution of these Fe species depends not only on the Fe content but also on the preparation method [7]. Different studies have presented different ways of preparing Fe/ZSM-5. These include chemical vapor deposition (CVD) of $FeCl_3$ [5,8,9,27], conventional liquid ion exchange [23,28], improved liquid ion exchange using $Fe(acac)_3$ [6] and Fe^{2+} ion generated by iron powder [4,29], and hydrothermal synthesis [12,16]. Of these, CVD of $FeCl_3$, developed by Sachtler's group [8], is a superior method for obtaining high-loaded and high-dispersed Fe species in a reproducible manner.

Meanwhile, to enhance the reactivity of the catalysts, a high temperature treatment under reducing conditions has been suggested [15,30]. In this treatment, smaller fragments can be created by breaking the iron oxide clusters apart. These smaller fragments stabilize themselves by forming strong bonds with the zeolite matrix and do not agglomerate during reoxidation, resulting in increased catalytic activity [15,31]. This reductive high temperature treatment, called reductive solid-state ion exchange (RSIE), is one of the most effective ion exchange methods for In/ZSM-5 [32], Ga/ZSM-5 [33], and Ce/ZSM-5 [34], which are difficult to obtain in a highly dispersed state by the conventional liquid ion exchange method because of their higher cationic charges and/or larger hydration radii.

In this study, we obtained a series of Fe/ZSM-5 containing different types of Fe species by various preparation methods and Fe loading. The purpose of this paper is to identify active Fe species in SCR of NO by NH_3 and to quantify it under the coexistence of several Fe species. To achieve this ultimate goal, we apply several spectroscopic characterizations (X-ray diffraction (XRD) and UV–vis, Mössbauer, and FT-IR spectroscopies), and we introduce temperature-programmed desorption techniques using NH_3 (NH_3-TPD) and NO_2 (NO_2-TPD) to quantitative analysis of the adsorption sites. The important points to identify the active sites are, first, to apply the combination of several characterization techniques in case their sensitivities for each Fe species differ and, second, to investigate the correlation between these Fe species and their catalytic activities.

2. Experimental

2.1. Catalysts preparation

A series of Fe/ZSM-5 catalysts was prepared by impregnation (Imp), RSIE, and CVD with various levels of Fe loading. The sample coding was $Fe(x)_{met.}$, with x and met. being the Fe/Al molar ratio and the specific method (Imp, RSIE, or CVD), respectively.

The starting zeolite was NH_4-ZSM-5 (Tosoh HSZ-830NHA, $Si/Al_2 = 28$, $S_{BET} = 350\ m^2/g$). NH_4-ZSM-5 was transformed to H-ZSM-5 by calcining at 873 K in air for 5 h. $Fe(NO_3)_3{\cdot}9H_2O$ (Wako, >99%) and $FeCl_3$ (Wako, >99%) were used as Fe precursors.

For Imp method, the required amount of an aqueous $Fe(NO_3)_3{\cdot}9H_2O$ solution to obtain the desired Fe content was dropped onto H-ZSM-5 at 353 K. The water was allowed to slowly evaporate at 373 K and the solid was dried at 383 K. The sample was then calcined at 923 K in 20% O_2/N_2 for 5 h.

Table 1
Description of Fe/ZSM-5 catalysts.

Catalyst	Preparation method	Fe content[a]	
		[Fe/Al molar ratio]	[mmol/g]
$Fe(0.25)_{Imp}$	Impregnation	0.25	0.27
$Fe(0.50)_{Imp}$	Impregnation	0.50	0.54
$Fe(1.00)_{Imp}$	Impregnation	1.00	1.03
$Fe(0.25)_{RSIE}$	Reductive solid-state ion exchange	0.25	0.27
$Fe(0.50)_{RSIE}$	Reductive solid-state ion exchange	0.50	0.54
$Fe(1.00)_{RSIE}$	Reductive solid-state ion exchange	1.00	1.03
$Fe(0.29)_{CVD}$	Chemical vapor deposition	0.29	0.32
$Fe(0.44)_{CVD}$	Chemical vapor deposition	0.44	0.48
$Fe(0.78)_{CVD}$	Chemical vapor deposition	0.78	0.81

[a] Analyzed by ICP.

For RSIE method, Fe/ZSM-5 materials prepared by Imp method described above were placed in a flow reactor, heated to 923 K at 5 K/min in a flowing mixture of 5% H_2/N_2, and maintained them at this temperature for 5 h. The sample was then calcined at 923 K in 20% O_2/N_2 for 5 h.

CVD of $FeCl_3$ to H-ZSM-5 was conducted by modifying the sublimation method developed in Sachtler's group [8]. First, H-ZSM-5 was placed in the flow reactor and calcined in N_2 at 923 K to remove the residual water adsorbed on the surface. The calcined H-ZSM-5 was transferred to a glove box without contacting air and mechanically mixed with the appropriate amount of $FeCl_3$ required for the desired Fe loading. While still in the glove box, we placed this mixture into a sealed reactor, removed the reactor from the glove box, and set it in a furnace. Both H-ZSM-5 and $FeCl_3$ were heated to 923 K at 5 K/min in N_2 and maintained at this temperature for 2.5 h. At this point, $FeCl_3$ was sublimed into the cavities of H-ZSM-5 where it chemically reacts with the acid sites according to the reaction: $FeCl_3\ (g) + H^+_{zeol} \rightarrow [FeCl_2]^+_{zeol} + HCl\ (g)$. In this process, the sublimation temperature affects the nature and the distribution of Fe species. Krishna et al. [5] reported that high temperature (973 K) sublimation leads to more active NO reduction by NH_3 than low temperature (593 K) sublimation. We cooled the $[FeCl_2]^+_{zeol}$ loaded sample to room temperature, washed it with deionized water twice to replace chloride ions with hydroxide ions, and dried it at 383 K. Finally, the sample was calcined at 923 K in 20% O_2/N_2 for 5 h.

Fe content of all the samples was determined by inductively coupled plasma (ICP) analysis, and is presented in Table 1.

2.2. Catalytic activity tests

The SCR of NO by NH_3 was carried out in a fixed-bed flow reactor operating at atmospheric pressure. The reaction temperature was controlled using a programmable temperature controller. Reactant gases were a mixture consisting of 0.1% NO, 0.1% NH_3, 8% O_2, 10% CO_2, 8% H_2O, and the balance of N_2. The catalyst weight was 1.0 g and the total flow rate was 5 l/min. The NO_x concentration was continually monitored using a chemiluminescent NO_x analyzer. NO_x conversion was obtained from the difference in the NO_x concentrations before and after the SCR reaction under steady-state conditions. In addition, no formation of N_2O was observed in any samples during the reaction using a nondispersive infrared N_2O analyzer.

2.3. Catalysts characterization

XRD was performed using a Rigaku Rint-2200 X-ray diffractometer. An XRD spectrum was recorded in the $5° < 2\theta < 50°$ range using Cu$K\alpha$ radiation and a scanning speed of 1.5°/min.

UV–vis spectra were recorded at ambient temperature on a JASCO V-560 spectrometer equipped with a diffuse reflectance accessory (ISV-469). $BaSO_4$ was used as the reference material. To reduce light absorption, we diluted Fe/ZSM-5 samples with $BaSO_4$ in a ratio of 1:3. The spectra were measured in reflectance mode and converted with the Kubelka–Munk function $F(R_\infty)$.

^{57}Fe Mössbauer spectra were measured on a constant acceleration spectrometer with ^{57}Co in an Rh matrix source at ambient temperature and calibrated the velocity scale using the standard magnetic sextuplet spectrum of a high-purity iron foil absorber. All the spectra were deconvoluted with calculated Mössbauer spectra consisting of Lorentzian-shaped lines. In case of quadrupole splitting or magnetic splitting, the line widths and the adsorption areas of the constituent lines were constrained equally.

NH_3-TPD and NO_2-TPD was carried out in a fixed-bed flow reactor equipped with a quadrupole mass spectrometer (QMS, ULVAC messmate-200). For NH_3-TPD, the samples (250 mg each) were activated at 923 K for 30 min in a flow of 5% O_2/He (300 ml/min) and then at 673 K for 15 min in a He flow and followed by cooling to 373 K. The samples then adsorbed NH_3 at 373 K for 30 min and were flushed with He for 30 min to remove any physically adsorbed NH_3. Desorption was carried out at a heating rate of 10 K/min from 333 to 933 K in a He flow (100 ml/min). Desorbed NH_3 was analyzed by QMS based on the mass signal ($m/e = 16$).

For NO_2-TPD, the samples (400 mg each) were activated at 873 K for 30 min in a flow of 5% O_2/He (300 ml/min) and then cooled to 373 K in a He flow. The samples adsorbed NO_2 at 373 K for 20 min and were then flushed with He for 20 min to remove any physically adsorbed NO_2. Desorption was carried out at a heating rate of 10 K/min from 323 to 873 K in a He flow (100 ml/min). The effluent gases from the reactor were mainly NO_2 at low temperature (<623 K) and NO and O_2 at high temperature (>623 K) due to the $NO_2 \leftrightarrow NO + \frac{1}{2}O_2$ equilibrium. We observed no formation of N_2 or N_2O by QMS. The NO_2 concentration was obtained using the intensity of $m/e = 46$ (I_{46}), and the NO concentration was obtained using I_{46} and the intensity of $m/e = 30$ (I_{30}) according to the following equation: $I_{30} - \alpha \times \beta \times I_{46}$, where α and β are a relative sensitivity of NO to NO_2 in I_{30} and a I_{30}/I_{46} fragmentation ratio about NO_2, respectively.

In situ FT-IR spectra were recorded using a NEXUS 670 (Nicolet) equipped with a diffuse reflectance optics accessory and a high-temperature cell. The total gas flow was maintained at 200 ml/min by mass flow controllers. Prior to adsorption measurements with NO_2, the catalyst samples were pretreated *in situ* at 923 K in a flow of 5% O_2/N_2 for 20 min and then cooled to 323 K. The NO_2 adsorption was carried out at 373 K in a flow of 0.2% NO_2/N_2 for 40 min. At this point, saturated adsorption of NO_2 was verified by the intensity of the spectrum. The samples were then cooled to 323 K in a flow of N_2. All the spectra were collected at 323 K in a flow of N_2 by accumulating 400 scans at a resolution of 4 cm^{-1}. To achieve quantification, we normalized the spectra by the intensity of zeolite framework bands (650–700 cm^{-1}) or zeolite overtone bands (1850–1900 cm^{-1}).

3. Results

3.1. Catalytic activity

Fig. 1 shows the NO_x conversions of the NH_3-SCR reaction as a function of reaction temperature over Fe/ZSM-5 and over pure H-ZSM-5. Clearly, the catalytic activity of NO_x reduction increased with increasing Fe content and with increasing reaction temperature. Although the catalysts prepared by Imp did not exhibit any significant activity, those prepared by RSIE showed high activities, indicating that the reductive high temperature treatment increases the active Fe species in a sample. Of all the catalysts, since $Fe(0.78)_{CVD}$ showed the highest SCR activity, CVD is the most effective preparation technique of the three methods. Fig. 1d shows the NO_x conversions at 523 K as a function of the Fe content. When Fe/Al > 0.4, the SCR activity decreased according to the sequence CVD > RSIE > Imp. Thus, the generation of active Fe species is strongly dependent on the preparation method.

3.2. XRD

Fig. 2 shows the XRD patterns of Fe/ZSM-5 and H-ZSM-5. All the Fe/ZSM-5 exhibited the typical lines of MFI framework, indicating that the structure of the MFI remained intact even after Fe loading. However, the intensity of the MFI framework decreased with increasing Fe content because of the higher X-ray absorption coefficient of Fe compounds.

In these patterns, small diffraction peaks appeared at 2θ values of 33.2°, 35.6°, 40.9°, and 49.5°, indicating an α-Fe_2O_3 phase with particle sizes larger than 3–5 nm. The intensity of these peaks increased with Fe content and depended on the preparation method according to the sequence Imp > RSIE > CVD. Since this order is opposite to that of the catalytic activity, the crystalline α-Fe_2O_3 is thought to contribute little to the SCR reaction.

Since the α-Fe_2O_3 peak intensity of $Fe(1.00)_{RSIE}$ was smaller than that of $Fe(1.00)_{Imp}$, the reductive high temperature treatment has the functions of diminishing crystalline size or decreasing α-Fe_2O_3 quantity. Pirngruber et al. [31] reported that reductive pretreatment in H_2 broke the iron oxide clusters into smaller units by EXAFS analysis.

3.3. UV–vis spectroscopy

UV–vis spectra of Fe/ZSM-5 are presented in Figs. 3(I)–3(III) where spectra of reference samples, α-Fe_2O_3 with different particle sizes (L: 0.15 μm; S: 0.05 μm), and H-ZSM-5 are also given (see Fig. 3(IV)). In Fe/ZSM-5, the spectral intensity increased with increasing Fe content, and the spectral shapes varied strongly with the preparation method, indicating that the distribution of Fe species is different.

The absorption of the UV region (<450 nm) may be due to $O \rightarrow Fe^{3+}$ ligand-to-metal charge-transfer (LMCT) transitions. The charge transfer occurs from the highest lying O 2p orbitals to the half-occupied Fe 3d orbitals ($t_{2g} \rightarrow e_g$ in O_h symmetry and $e \rightarrow t_2$ in T_d symmetry) [35]. Schwidder et al. [4] ascribed the band at <300 nm to isolated Fe^{3+}, the band at 300–400 nm to oligomeric clusters, and the band at >400 nm to large Fe_2O_3 particles. However, UV–vis cannot distinguish between isolated and binuclear Fe species as a strong shift of the LMCT bands is not expected [23].

On the other hand, the absorption of the visible region (>450 nm) may be due to d–d transitions, a phenomenon unique to α-Fe_2O_3 [3,25,26]. Lu et al. [26] ascribed the band near 865 nm to $^6A_1 \rightarrow {}^4T_1(^4G)$, the band near 670 nm to $^6A_1 \rightarrow {}^4T_2(^4G)$, and the band near 560 nm to $^6A_1 + {}^6A_1 \rightarrow {}^4T_1(^4G) + {}^4T_1(^4G)$. Here, $^6A_1$, $^4T_1(^4G)$, and $^4T_2(^4G)$ represent the ground state, the first excited state, and the second excited state configurations of high spin Fe^{3+}, respectively. In the above three absorptions, the band near 560 nm, the electron pair transition (EPT), is the strongest. The actual position of the EPT, however, depends on the particle size of α-Fe_2O_3 [25,26] as is evident from Fig. 3(IV).

In Figs. 3(I)–3(III), the specific difference in the spectral shape was the visible region (>450 nm) assigned to large α-Fe_2O_3 species, and their intensities follow the sequence Imp > RSIE > CVD, the same trend displayed be XRD. Thus, the proportion of other Fe species, oligometric clusters, and/or ion-exchanged oxo-Fe^{3+} should be in the contrary sequence (CVD > RSIE > Imp). However, it is difficult to quantify these species because the ex-

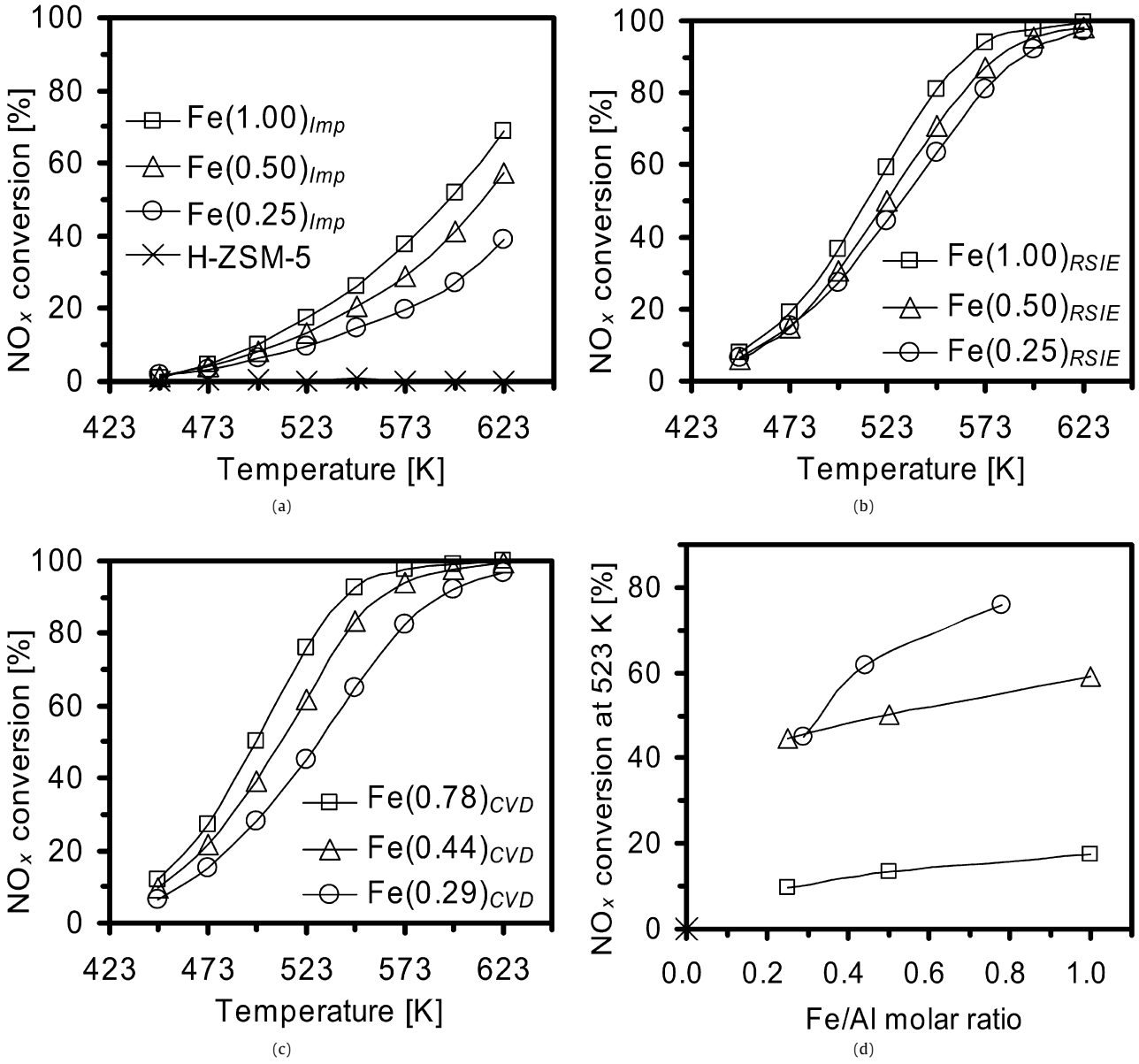

Fig. 1. Reaction temperature dependence of NO_x conversion over H-ZSM-5 and Fe/ZSM-5 prepared by (a) Imp, (b) RSIE, (c) CVD, and (d) NO_x conversion at 523 K as a function of Fe/Al molar ratio over (×) H-ZSM-5 and Fe/ZSM-5 prepared by (□) Imp, (△) RSIE, and (○) CVD. Reaction condition: 0.1% NO, 0.1% NH_3, 8% O_2, 10% CO_2, 8% H_2O, and balance of N_2, W/F = 0.2 gl/min.

tinction coefficients of each species are not known and because of the complex overlapping of several peaks.

3.4. ^{57}Fe Mössbauer spectroscopy

Fig. 4 shows ^{57}Fe Mössbauer spectra of $Fe(1.00)_{Imp}$, $Fe(1.00)_{RSIE}$, and $Fe(0.78)_{CVD}$. All the spectra can be deconvoluted into a hyperfine magnetic sextet line and two quadrupole doublet lines. The sextet line is ascribed to aggregated large α-Fe_2O_3 particles [36] and the doublet lines are ascribed to paramagnetic Fe^{3+} ions or superparamagnetic α-Fe_2O_3 with sizes less than 13.5 nm [18,19,36]. The hyperfine parameters of these spectra are given in Table 2 as along with the relative integrated intensity of each Fe species.

All the samples were mainly constituted by large α-Fe_2O_3 particles in the order $Fe(1.00)_{Imp} > Fe(1.00)_{RSIE} > Fe(0.78)_{CVD}$, which is the same trend observed in XRD and UV–vis results. The doublet line with isomer shifts of 0.32 mm/s and quadrupole splitting of 0.5–0.8 mm/s (doublet (I) in Table 2) might be small α-Fe_2O_3 particles in superparamagnetic states. On the other hand, the doublet line with isomer shifts of 0.32 mm/s and quadrupole splitting of 1.26 mm/s (doublet (II) in Table 2) might be Fe^{3+} in a strong, distorted octahedral environment, most likely oxo-Fe^{3+} ions at ion-exchanged sites or Fe_xO_y oligomers. Detailed classification of these species, however, is difficult from these spectra. Low temperature measurements applying high vacuum conditions are necessary to obtain additional information [12,19].

3.5. NH_3-TPD

NH_3-TPD spectra of Fe/ZSM-5 and H-ZSM-5 are presented in Fig. 5. For H-ZSM-5, two main peaks (both broad) were located around 473 and 723 K. The desorption peak at the lower temperature is assigned to physorbed NH_3, while the peak at the higher temperature is assigned to NH_3 strongly adsorbed on the Brønsted

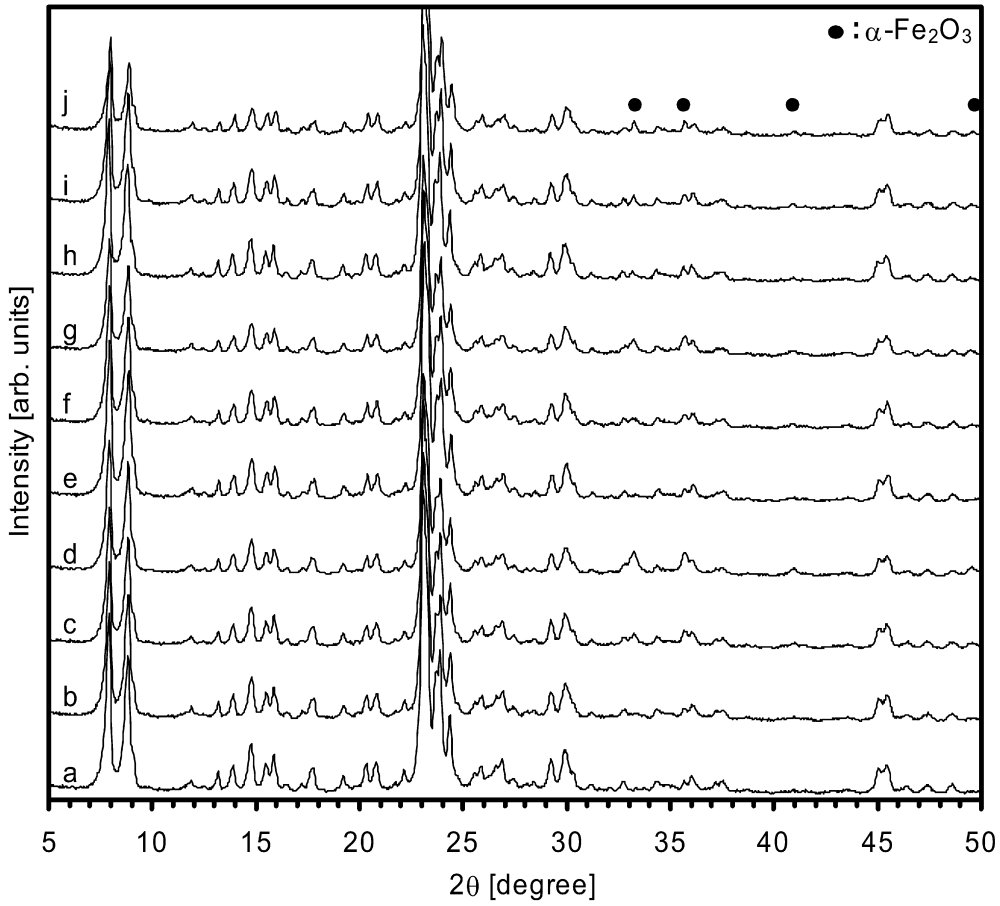

Fig. 2. XRD patterns over (a) H-ZSM-5, (b) $Fe(0.25)_{Imp}$, (c) $Fe(0.50)_{Imp}$, (d) $Fe(1.00)_{Imp}$, (e) $Fe(0.25)_{RSIE}$, (f) $Fe(0.50)_{RSIE}$, (g) $Fe(1.00)_{RSIE}$, (h) $Fe(0.29)_{CVD}$, (i) $Fe(0.44)_{CVD}$, and (j) $Fe(0.78)_{CVD}$.

acid sites [27,37]. For Fe/ZSM-5, the intensity of the higher temperature peak was lower than that of H-ZSM-5, because the Brønsted acid protons were substituted for Fe^{3+}.

Fig. 6 shows the comparison of the preparation methods. The loss in intensity of the higher temperature peak, attributed to Fe^{3+} ion exchange, follows the order CVD > RSIE > Imp and is consistent with UV–vis and ^{57}Fe Mössbauer results.

Interestingly, the intensity around 573 K increased as that of the higher temperature peak at 723 K decreased, suggesting that the ion-exchanged Fe^{3+} lead to the new acid sites. Sugawara et al. [38] reported similar NH_3 desorption at 573 K over Fe ion-exchanged Na/ZSM-5, whose intensity increased with increasing Fe content, and they have attributed this peak to desorption from binuclear Fe species. Generation of this new acid site can be supported by FT-IR data described later.

3.6. NO_2-TPD

NO_2-TPD spectra of Fe/ZSM-5 and H-ZSM-5 are presented in Fig. 7, in which the vertical axis is the concentration of NO_x. Two main peaks were found around 473 and 623 K, and the higher temperature (HT) peak increased with increasing Fe content. Furthermore, the preparation method influenced the intensity of the HT peak, according to the order CVD > RSIE > Imp, coinciding with the quantity of Fe^{3+} ion exchange in NH_3-TPD.

Long and Yang [37] have reported similar spectra in NO_x-TPD preadsorbed with NO and O_2. They have attributed the lower temperature peak to physisorbed NO_x and the higher temperature peak to chemisorbed NO_x bonded to Fe sites because the lower temperature peak was independent of Fe content and the higher temperature peak increased with Fe content.

To estimate the amount of NO_x desorption in the HT peak, we carried out curve fitting. Fig. 7(IV) shows the fitted spectra of $Fe(0.78)_{CVD}$, and Table 3 lists the quantities. The NO_x desorption amount is much smaller than the Fe content, indicating that the HT peak is probably due to desorption from specific minority Fe sites (see Section 4). In fact, taking $Fe(0.78)_{CVD}$ as an example, the ratio of the NO_x desorption amount to the Fe content (NO_x/Fe) in Table 3 is smaller than the proportion of doublet (II) in Table 2 which is considered to be the mixture of ion-exchanged oxo-Fe^{3+} and Fe_xO_y oligomers.

3.7. In situ FT-IR spectroscopy

Fig. 8 shows FT-IR spectra of the –OH stretching region before and after NO_2 adsorption over $Fe(0.78)_{CVD}$ and H-ZSM-5. Five peaks (3783, 3745, 3676, 3662, 3610 cm^{-1}) were observed over $Fe(0.78)_{CVD}$. The peaks at 3783, 3745, 3662, and 3610 cm^{-1} were also observed in the spectra of H-ZSM-5. The peaks at 3745, 3662, and 3610 cm^{-1} were assigned to the terminal silanols (terminal Si–OH), –OH groups associated with extra-framework aluminum (ex Al–OH), and bridging –OH groups (i.e., the Brønsted acid sites), respectively [14,39,40]. The 3783 cm^{-1} band has been assigned to a hydroxyl group attached to a tri-coordinated aluminum atom linked to the network via two oxygen bonds (tri Al–OH) [14,39].

In $Fe(0.78)_{CVD}$, the 3610 cm^{-1} band intensity was much lower than that of H-ZSM-5, and a new band appeared at 3676 cm^{-1}. These bands are direct evidence for the replacement of the Brønsted acid sites by Fe^{3+} species and for the formation of the OH

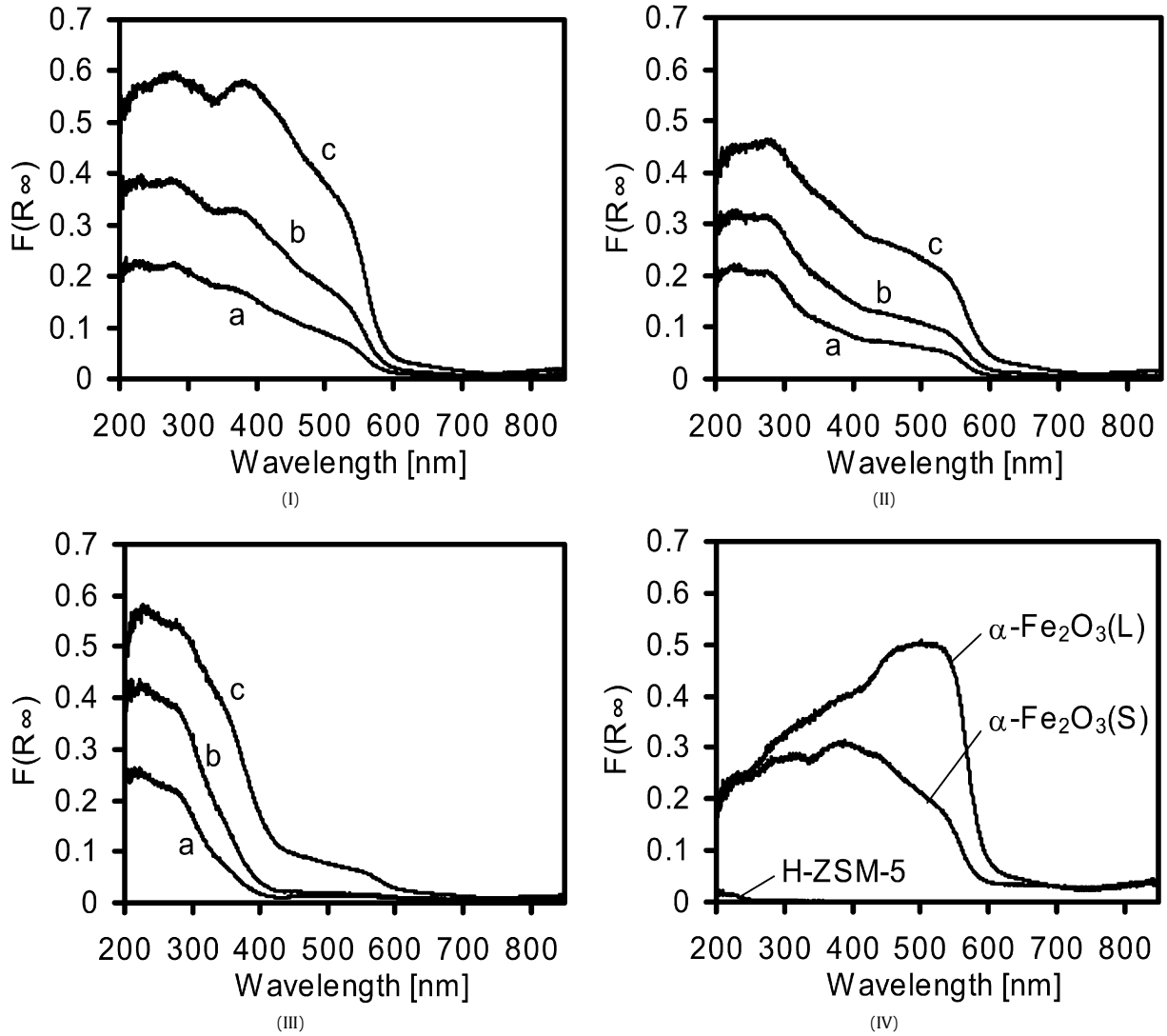

Fig. 3. UV–vis spectra over Fe/ZSM-5 prepared by (I) Imp (a: $Fe(0.25)_{Imp}$, b: $Fe(0.50)_{Imp}$, and c: $Fe(1.00)_{Imp}$); (II) RSIE (a: $Fe(0.25)_{RSIE}$, b: $Fe(0.50)_{RSIE}$, and c: $Fe(1.00)_{RSIE}$); (III) CVD (a: $Fe(0.29)_{CVD}$, b: $Fe(0.44)_{CVD}$, c: $Fe(0.78)_{CVD}$) as compared with reference spectra (IV) α-Fe_2O_3 with different particle size (L; 0.15 μm, S; 0.05 μm) and H-ZSM-5.

group linked with Fe^{3+} species (Fe–OH) [39,40], facts which are consistent with the above NH_3-TPD data. After the NO_2 adsorption, only the 3783 cm^{-1} band decreased over H-ZSM-5 while the 3676 cm^{-1} band also decreased over $Fe(0.78)_{CVD}$, indicating that NO_2 adsorbed on the Fe–OH sites. This adsorption could be observed in the NO_x stretching region, as shown below.

Fig. 9 shows the difference of the spectra before and after NO_2 adsorption in the NO_x stretching region. In H-ZSM-5, small bands at 1656 and 1590 cm^{-1} and a very weak broad band at 2135 cm^{-1} were observed. These bands at 2135, 1656, and 1590 cm^{-1} could be assigned to NO^+, the nitro group (NO_2), and nitrate ions attached to H-ZSM-5, respectively [13,22,41]. In Fe/ZSM-5, new bands at 1635 and 1572 cm^{-1} were observed in addition to the above bands. The bands at 1635 and 1572 cm^{-1} are assigned to the nitro and nitrate groups adsorbed on Fe species, respectively [22,41]. By considering the fact that Fe–OH band decreased with NO_2 adsorption (see Fig. 8), NO_2 must have adsorbed on ion-exchanged Fe^{3+} sites.

The change of spectra caused by NO_2 adsorption was also confirmed in the zeolite framework T–O–T vibration region, as shown in Fig. 10. Bands in the 850–750 cm^{-1} region have been attributed to both internal and external symmetric vibrations that have not been affected by ion exchange or NO_2 adsorption [13,41,42]. On the other hand, bands in the 1000–850 cm^{-1} range, typical for transition metal exchanged zeolites [42,43], have been attributed to the perturbation of the internal asymmetric T–O–T vibrations by Fe^{3+} located at zeolite ion exchange sites. (Unperturbed ring bands appeared in the 1120–1020 cm^{-1} region.) In fact, the perturbation bands increased with Fe content and depended on the preparation method according to the order CVD > RSIE > Imp, data in reasonable agreement with UV–vis, and ^{57}Fe Mössbauer spectroscopies, and with the NH_3-TPD results.

The perturbation band position shifted to lower wave numbers after NO_2 adsorption with almost no change in intensity. It has been reported that the perturbation band position depends on the Fe oxidation state and adsorption of substance [13,41–43]. Gao et al. [41] and Mauvezin et al. [42] have reported that the perturbation band shifted to higher wave numbers upon reducing the pre-oxidized Fe/ZSM-5, and that this shift was caused by the reduction of Fe^{3+} and by change of its coordination. In addition, Gao et al. [41] have observed that the perturbation band shifted slightly to lower wave numbers by $NO + O_2$ adsorption, possibly indicating that the Fe oxidation state was higher than that of the pre-oxidized Fe/ZSM-5. Nobukawa et al. [39] and Jia et al. [44] have observed the $Fe^{(3+\delta)+}$ sites over Fe/ZSM-5 after N_2O treatment (an oxidation state higher than that after O_2 treatment) by XAFS study. Based on these reports, the oxidation and/or coordination states of Fe were changed by NO_2 adsorption.

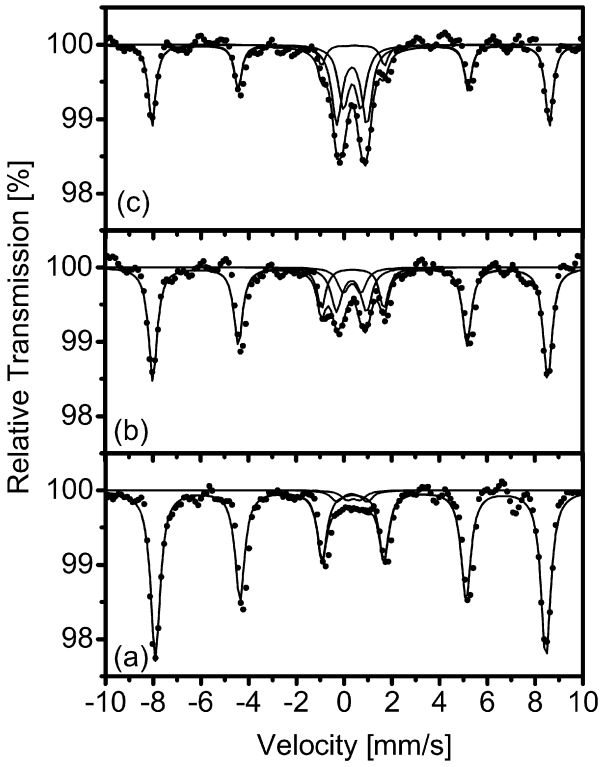

Fig. 4. ^{57}Fe Mössbauer spectra at ambient temperature over (a) Fe(1.00)$_{Imp}$, (b) Fe(1.00)$_{RSIE}$, and (c) Fe(0.78)$_{CVD}$. Curve fitting results are listed in Table 2.

Table 2
^{57}Fe Mössbauer hyperfine parameters and relative integrated intensities of Fe(1.00)$_{Imp}$, Fe(1.00)$_{RSIE}$, and Fe(0.78)$_{CVD}$.

Catalyst	Identification	Isomer shift [mm/s]	Quadrupole splitting [mm/s]	Hyperfine field [kOe]	Relative intensity [%]
Fe(1.00)$_{Imp}$	Sextet	0.37	−0.1	506	95
	Doublet (I)	0.39	0.55	–	2
	Doublet (II)	0.32	1.26	–	3
Fe(1.00)$_{RSIE}$	Sextet	0.37	−0.1	515	78
	Doublet (I)	0.34	0.74	–	8
	Doublet (II)	0.32	1.26	–	14
Fe(0.78)$_{CVD}$	Sextet	0.37	−0.1	515	52
	Doublet (I)	0.34	0.74	–	21
	Doublet (II)	0.32	1.26	–	27

4. Discussion

4.1. Fe species in Fe/ZSM-5

According to XRD and UV–vis and Mössbauer spectroscopies, all the catalysts contained aggregated α-Fe_2O_3, and their relative concentrations were Imp > RSIE > CVD. In addition, we also identified Fe_xO_y oligomer and oxo-Fe^{3+} (following the order CVD > RSIE > Imp). From NH_3-TPD and FT-IR study, we confirmed the substitution of Brønsted acid protons by Fe^{3+}, and its degree was in rough agreement with the trend of the oxo-Fe^{3+} identified by UV–vis and Mössbauer spectroscopies. Consequently, in the Fe/ZSM-5 catalysts, three types of Fe species coexist, aggregated α-Fe_2O_3 particles, Fe_xO_y oligomer in the extra-framework, and oxo-Fe^{3+} at ion-exchanged sites.

When quantifying these Fe species, it should be noted that the relative intensity of the signals in the spectra do not necessarily reflect the proportion of Fe species correctly. Comparing between Mössbauer and UV–vis spectroscopy, for instance, α-Fe_2O_3 was a major species in Mössbauer results (see the relative intensity of magnetic sextet line in Fig. 4), while it was minor in UV–vis results (see the relative intensity of $\lambda > 450$ nm in Fig. 3). The reason for this discrepancy is explained as follows: UV–vis spectroscopy tends to underestimate large α-Fe_2O_3 particles because of their surface-sensitive character and the extinction coefficients of each species may be different. On the other hand, Mössbauer spectroscopy tends to overestimate α-Fe_2O_3 species because the Debye temperature of α-Fe_2O_3 particles is significantly higher than that of oxo-Fe^{3+} and oligomers, leading to decreasing the fraction of recoil-free absorption [45]. Thus, UV–vis is sensitive to disperse structures while Mössbauer spectroscopy is sensitive to large aggregates. To avoid erroneous conclusions because of this differ-

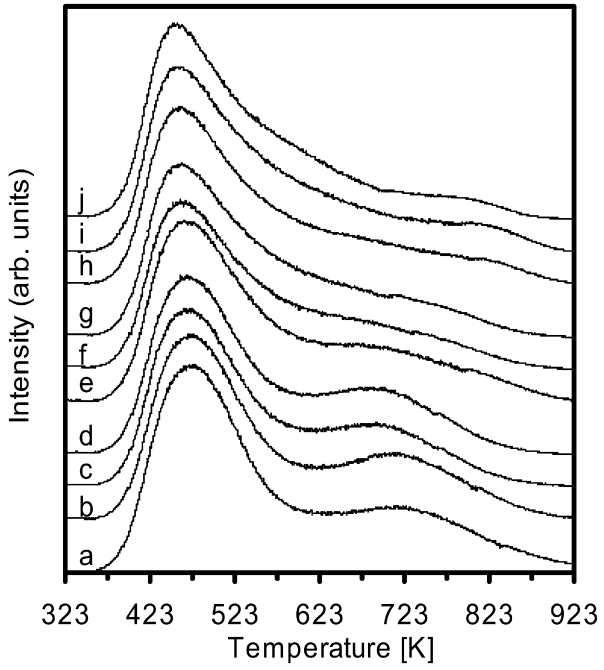

Fig. 5. Temperature-programmed desorption of NH_3 over (a) H-ZSM-5, (b) Fe(0.25)$_{Imp}$, (c) Fe(0.50)$_{Imp}$, (d) Fe(1.00)$_{Imp}$, (e) Fe(0.25)$_{RSIE}$, (f) Fe(0.50)$_{RSIE}$, (g) Fe(1.00)$_{RSIE}$, (h) Fe(0.29)$_{CVD}$, (i) Fe(0.44)$_{CVD}$, and (j) Fe(0.78)$_{CVD}$. Catalyst weight: 250 mg, NH_3 adsorption: 373 K for 30 min, measurement conditions: He flow at 100 ml/min, heating rate: 10 K/min from 333 to 933 K.

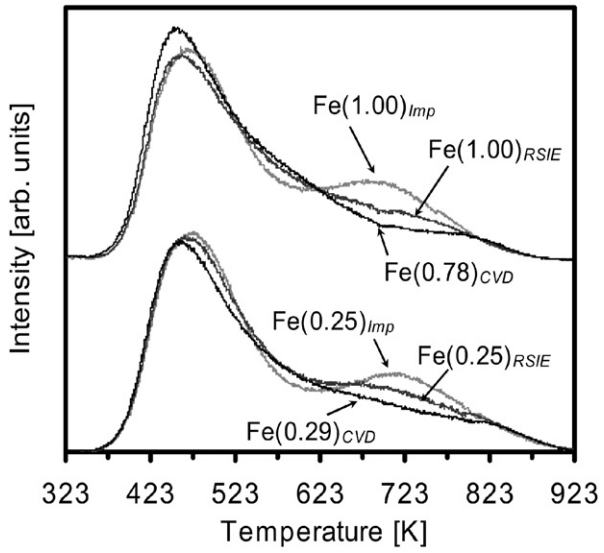

Fig. 6. Temperature-programmed desorption of NH_3 over Fe/ZSM-5 compared with preparation method. Conditions are same as Fig. 5.

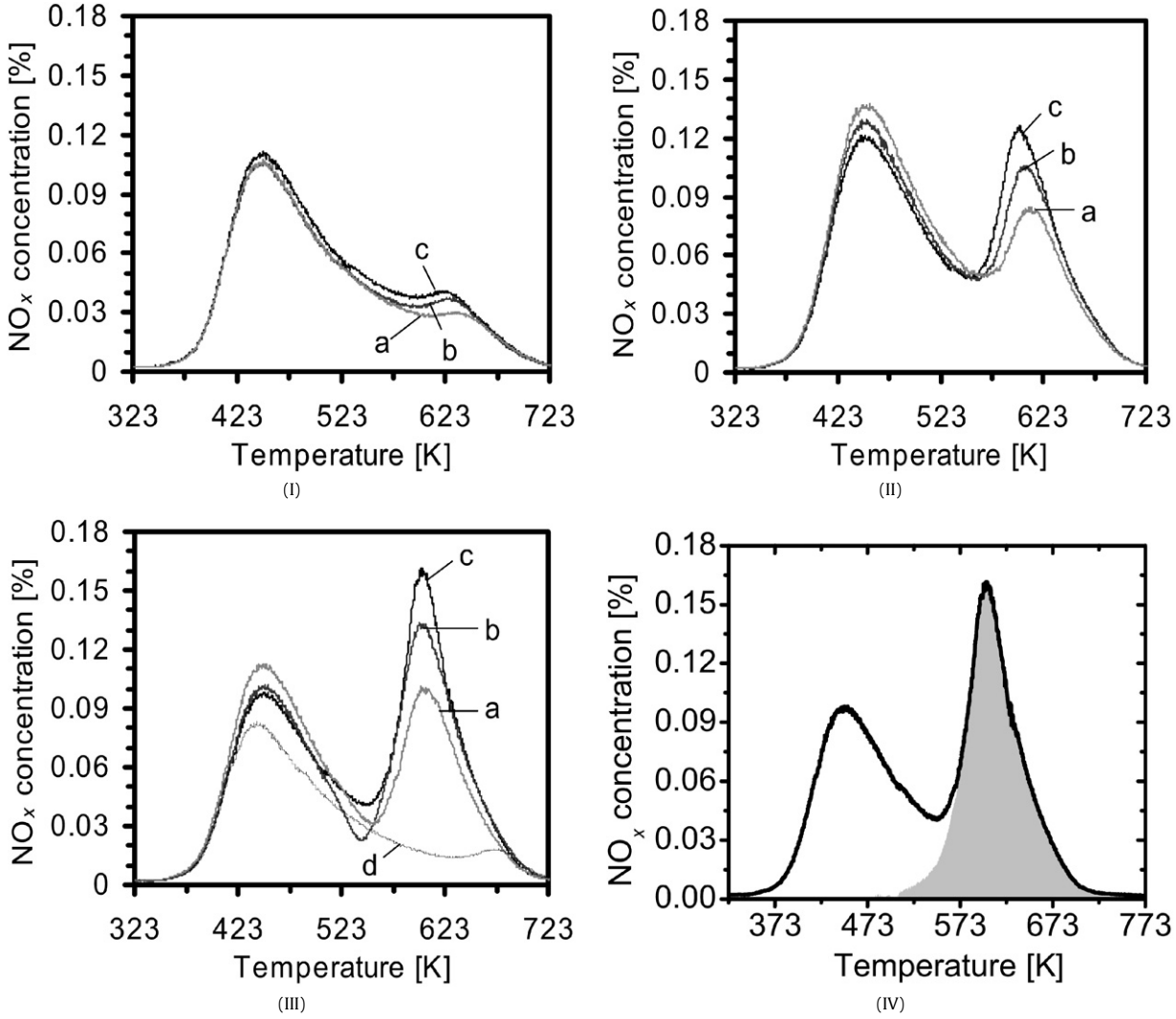

Fig. 7. Temperature-programmed desorption of NO_2 over Fe/ZSM-5 prepared by (I) Imp (a: $Fe(0.25)_{Imp}$, b: $Fe(0.50)_{Imp}$, and c: $Fe(1.00)_{Imp}$); (II) RSIE (a: $Fe(0.25)_{RSIE}$, b: $Fe(0.50)_{RSIE}$, and c: $Fe(1.00)_{RSIE}$); (III) CVD (a: $Fe(0.29)_{CVD}$, b: $Fe(0.44)_{CVD}$, c: $Fe(0.78)_{CVD}$) and d: H-ZSM-5; and (IV) Curve fitting spectra of $Fe(0.78)_{CVD}$. Catalyst weight: 400 mg, NO_2 adsorption: 373 K for 20 min, measurement conditions: He flow at 100 ml/min, heating rate: 10 K/min from 323 to 873 K.

Table 3
NO_x desorption amount at the higher temperature peak in NO_2-TPD.

Catalyst	NO_x desorption[a]		
	Amount [μmol/g]	Ratio to Fe content [NO_x/Fe]	Ratio to Al content [NO_x/Al]
H-ZSM-5	19	–	0.02
$Fe(0.25)_{Imp}$	34	0.12	0.03
$Fe(0.50)_{Imp}$	41	0.08	0.04
$Fe(1.00)_{Imp}$	48	0.05	0.05
$Fe(0.25)_{RSIE}$	82	0.31	0.08
$Fe(0.50)_{RSIE}$	96	0.18	0.09
$Fe(1.00)_{RSIE}$	110	0.11	0.11
$Fe(0.29)_{CVD}$	92	0.29	0.09
$Fe(0.44)_{CVD}$	116	0.24	0.11
$Fe(0.78)_{CVD}$	126	0.16	0.12

[a] Higher temperature peak in NO_2-TPD.

ence in sensitivity, not only the combination of several spectroscopies but also adsorption and desorption analyses using proper molecules are necessary.

Regarding the structure of oxo-Fe^{3+} at ion-exchanged sites, the binuclear Fe–O–Fe complexes have been suggested from EXAFS studies by several group [18,20,21]. On the other hand, mononuclear sites or nanoclusters with an average composition of Fe_4O_4 have also been identified [4,7]. In our characterization study, although it was not possible to predict the structure of oxo-Fe^{3+} species, we clearly confirmed the degree of Fe^{3+} ion exchange by NH_3-TPD (Fig. 6) and FT-IR (Figs. 8 and 10). In addition, the HT peak observed in NO_2-TPD (Fig. 7) probably originated at some specific Fe sites. Its detailed identification and the relation with the catalytic activity are discussed below.

4.2. Correlation between active Fe sites and catalytic activity

To determine the origin of the HT peak in NO_2-TPD, we investigated its relation with the degree of ion exchange, estimating this degree by the T–O–T perturbation peak in FT-IR (Fig. 10) because of its high accuracy compared with that in the –OH stretching region (Fig. 8) or in NH_3-TPD (Fig. 7). To estimate the degree of ion exchange, the deconvolution of the T–O–T perturbation peak was carried out, fitting the peak with a Gaussian line-shape after subtracting the background (Fig. 11). Fig. 12 shows the relation between the T–O–T perturbation peak and the NO_x amount at the HT peak. Clearly, the NO_x amount correlates with the T–O–T perturbation peak, indicating that the HT peak should mainly be ascribed to desorption from ion-exchanged oxo-Fe^{3+} sites. In other wards, NO_2 adsorbed selectively on oxo-Fe^{3+} sites. In general, NO_2 strongly interact with oxygen defect sites in metal-oxide [46]. In addition,

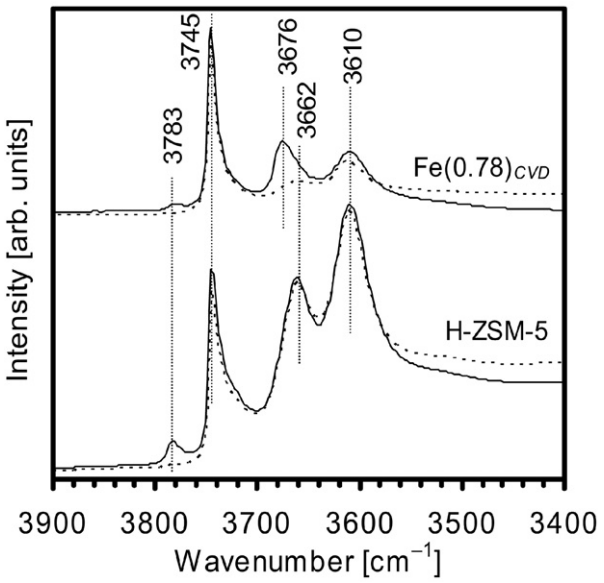

Fig. 8. FT-IR spectra of OH stretching region before (full lines) and after (dotted lines) NO_2 adsorption over $Fe(0.78)_{CVD}$ and H-ZSM-5. Pretreatment: 5% O_2/N_2 for 20 min at 923 K, NO_2 adsorption: 0.2% NO_2/N_2 for 40 min at 373 K, measurement conditions: 323 K in N_2 flowing.

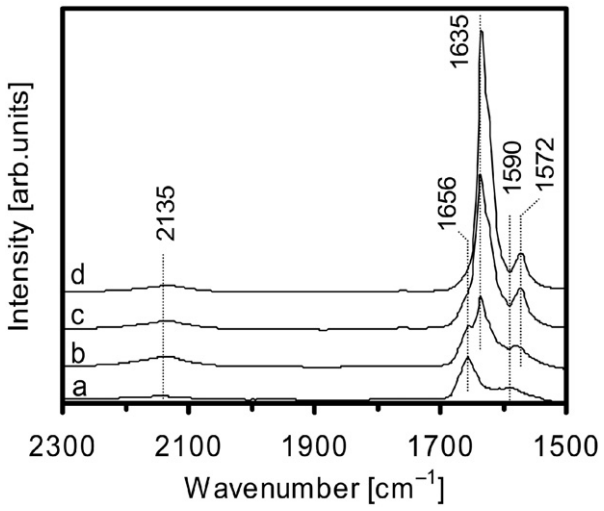

Fig. 9. Difference FT-IR spectra between before and after NO_2 adsorption in the NO_x stretching region over (a) H-ZSM-5, (b) $Fe(1.00)_{Imp}$, (c) $Fe(1.00)_{RSIE}$, and (d) $Fe(0.78)_{CVD}$. Measurement and NO_2 adsorption conditions are same as Fig. 8.

considering the report that binuclear oxo-Fe^{3+} have vacancy sites on which NO and H_2O can adsorb [10,18], our result of NO_2 selective adsorption onto oxo-Fe^{3+} is valid.

Fig. 13 shows the relationships between the NO_x amount and NO_x conversion at 523 K. NO_x conversion has a excellent linear correlation with the NO_x desorption amount, suggesting that the ion-exchanged oxo-Fe^{3+} are the active sites for the NH_3-SCR reaction.

Here, H-ZSM-5 has not exhibited any catalytic activity in this temperature range whereas its amount of NO_x desorption at the HT peak is a non-zero value. We can assume that the HT peak in H-ZSM-5 is due to desorption from the zeolite defect sites (tri Al–OH) that are observed in the –OH stretching region at 3783 cm^{-1} (see Fig. 8). These sites are known to possess not only the Lewis acid but also basic properties [47], permitting NO_x desorption at higher temperatures. By subtracting the defect sites, we obtain the number of active sites $N_{act.}$, such that $N_{act.} = N_{Fe/ZSM\text{-}5} - N_{H\text{-}ZSM\text{-}5}$, where $N_{Fe/ZSM\text{-}5}$ and $N_{H\text{-}ZSM\text{-}5}$ are the NO_x amount of the HT peak of Fe/ZSM-5 and H-ZSM-5, respectively.

The amount of active sites provides the turnover frequency (TOF) for the NH_3-SCR reaction. Fig. 14 shows TOF as a function of the active site amount, indicating that TOF is almost constant and suggesting that it is not affected by the preparation method.

Since the active site amount was much lower than the total Fe content, the active sites are a minority species, and the remaining Fe species barely modify the catalytic activity. As we have mentioned in the previous section, it was not possible to predict the structure of ion-exchanged species. Assuming that more than one structure exists (like isolate and binuclear), however, one can expect that either (I) all the structures assigned to active sites possess a same TOF value and the non-active structures, if any, have a near zero TOF, or (II) the distribution of each structure is identical in all the catalysts.

Kumar et al. [48] have reported that there are three types of ion-exchanged isolated sites in addition to oligonuclear clusters (which include ion-exchanged binuclear in their paper) and Fe oxide aggregates characterized by UV–vis and EPR. They have proposed that one of the isolated sites is probably active for SCR by isobutene and NH_3. At the same time, oligonuclears (probably include binuclear) contribute to the reactions as well, and the relative concentration between isolates and oligonuclears has been varied with total Fe content [48], indicating that the possibility of (II) described above is ruled out. In addition, they have reported that oligonuclears (and aggregates) are more active in the unselective oxidation of the reductant [48]. In our study, the unselective oxidation of NH_3 did not occurred because of low temperature measurement (<650 K). Considering the sharp and highly symmetric NO_2 desorption peak (Fig. 7(IV)), even if there are several active sites, their contribution to the low-temperature SCR should be in the same level (i.e. possibility (I) described above), and they should have similar characteristics. In fact, there are some common features between the active isolated species and oligonuclears in Kumar's report [48]; their EPR signals are appeared at $g' \approx 2$ (other isolates are appeared at $g' \approx 4.3$ and 6), and they have higher reduction-resistance compared to other isolates. For further detailed discussion about ion-exchanged structures, however, it is needed to prepare the catalysts exclusively containing ion-exchanged species [4,21,23] and to apply more elaborate characterizations; extremely low temperature Mössbauer using ^{57}Fe-enriched samples [49], Kβ-detected XAFS [50], magnetization measurement [23], *in situ* EPR [48], etc.

Fig. 15 shows the Arrhenius plot of the logarithm of TOF against the inverse temperature (523–473 K). From this slope, we obtained an apparent activation energy E_a of 46 kJ/mol. This value is close to the value found by Devadas et al. for Fe/ZSM-5 (45 kJ/mol) [51]. Thus, the estimation of the active sites and TOF in this work is a reasonable and reliable value.

5. Conclusions

We prepared Fe/ZSM-5 catalysts by several methods (Imp, RSIE, and CVD) with various levels of Fe loading and tested their catalytic activities in SCR of NO by NH_3. The SCR activity was more dependent on the preparation method than on the Fe loading, according to the order CVD > RSIE > Imp. As determined by several characterization methods, three types of Fe species are found to coexist—aggregated α-Fe_2O_3 particles, Fe_xO_y oligomer in the extra-framework, and oxo-Fe^{3+} at ion-exchanged sites—and their distribution is strongly dependant on the preparation method. UV–vis and Mössbauer spectroscopies were the most useful techniques for investigating the type of Fe species contained in the samples; however, accurate quantifications were difficult due to their different sensitivities for each Fe species. Although NH_3-TPD and FT-IR pro-

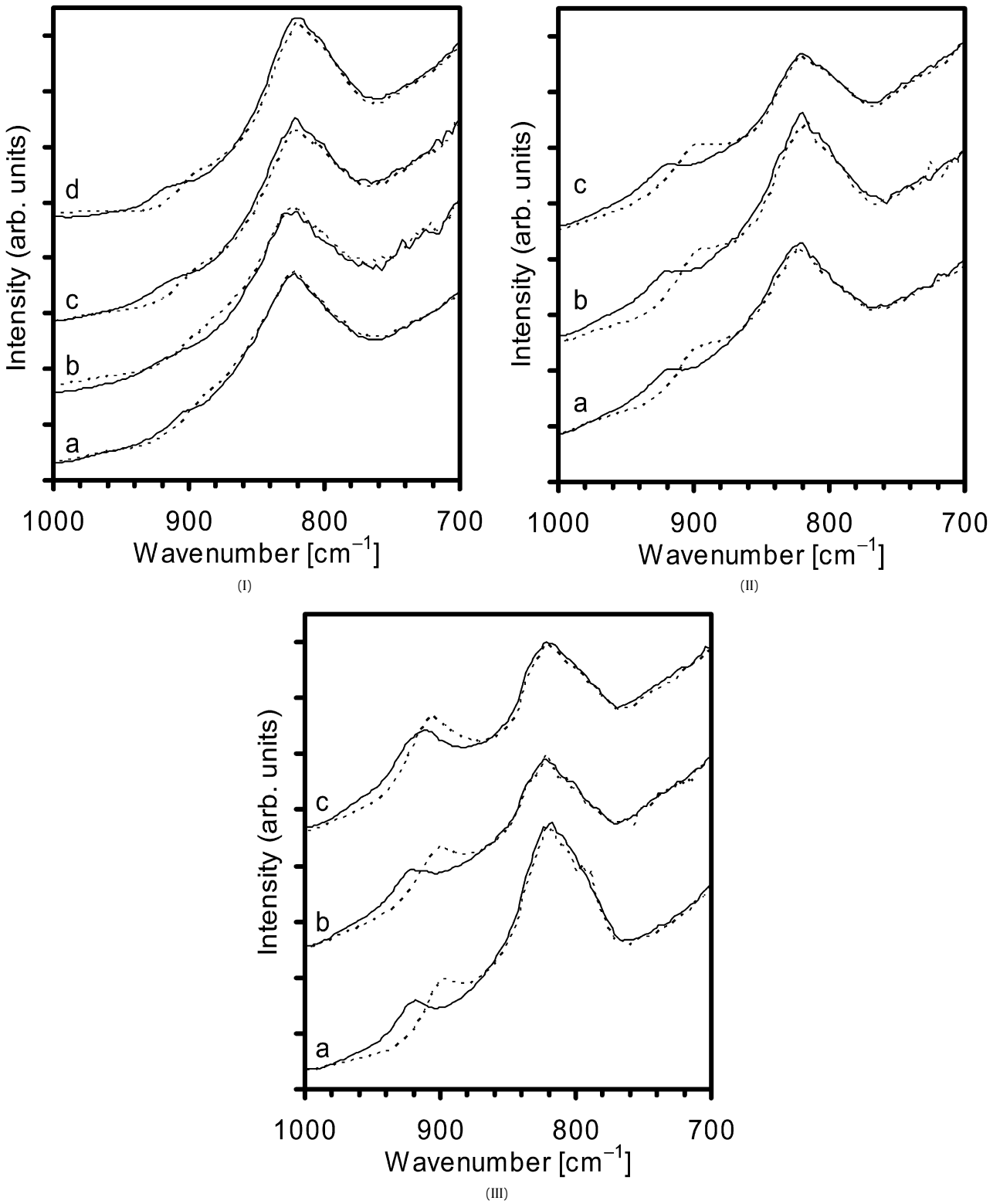

Fig. 10. FT-IR spectra of zeolite framework T–O–T vibration region before (full lines) and after (dotted lines) NO_2 adsorption over (I)-a H-ZSM-5 and Fe/ZSM-5 prepared by (I) Imp (b: $Fe(0.25)_{Imp}$, c: $Fe(0.50)_{Imp}$, and d: $Fe(1.00)_{Imp}$); (II) RSIE (a: $Fe(0.25)_{RSIE}$, b: $Fe(0.50)_{RSIE}$, and c: $Fe(1.00)_{RSIE}$); and (III) CVD (a: $Fe(0.29)_{CVD}$, b: $Fe(0.44)_{CVD}$, c: $Fe(0.78)_{CVD}$). Measurement and NO_2 adsorption conditions are same as Fig. 8.

vided ion exchange information at Brønsted acid sites, they did not yield accurate quantifications. For NO_2-TPD, which had two NO_x desorption peaks, its HT peak correlated with the T–O–T perturbation peak in FT-IR, indicating that the HT peak was due to desorption from ion-exchanged oxo-Fe^{3+} sites. Since the HT peak had a linear relationship with the catalytic performance, the ion-exchanged sites should be the active sites and TOF is not altered by the preparation method and Fe loading.

Based on this study, we can state that NO_2-TPD enables us to quantify the active sites despite the coexistence of several Fe species and is a powerful technique because of its easy acquisition and high accuracy.

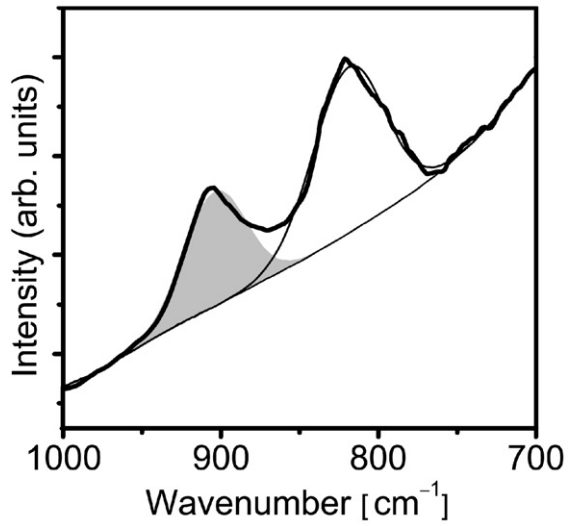

Fig. 11. The result of the deconvolution of the T–O–T perturbation peak over Fe(0.78)$_{CVD}$. The peak was fitted using Gaussian line shapes after subtracting the background.

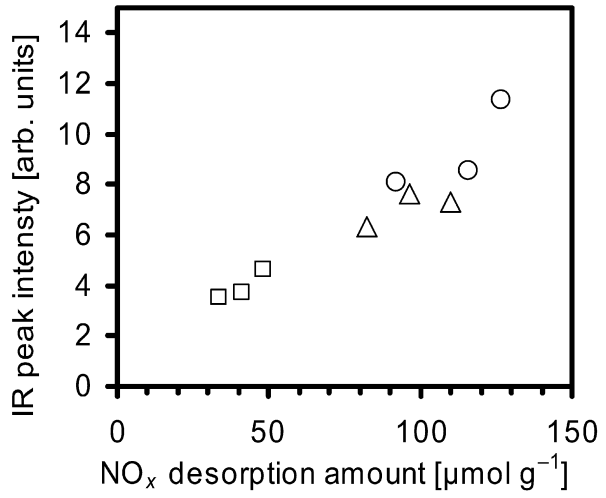

Fig. 12. Relation between the T–O–T perturbation peak and the NO_x amount at the HT peak in NO_2-TPD for (×) H-ZSM-5 and Fe/ZSM-5 prepared by (□) Imp, (△) RSIE, and (○) CVD.

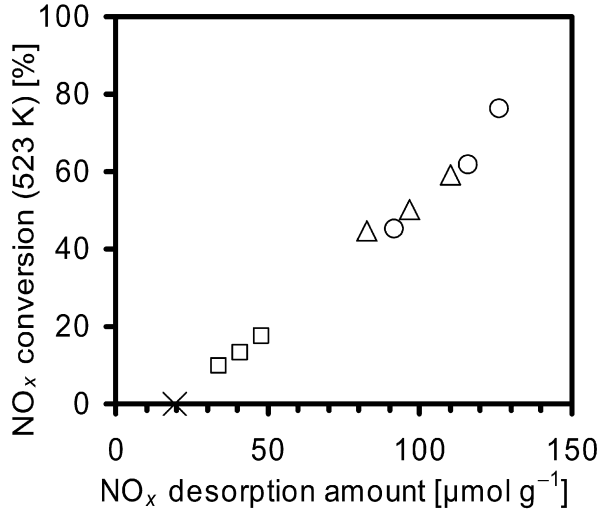

Fig. 13. Relation between the NO_x amount at the HT peak and NO_x conversion at 523 K for (×) H-ZSM-5 and Fe/ZSM-5 prepared by (□) Imp, (△) RSIE, and (○) CVD.

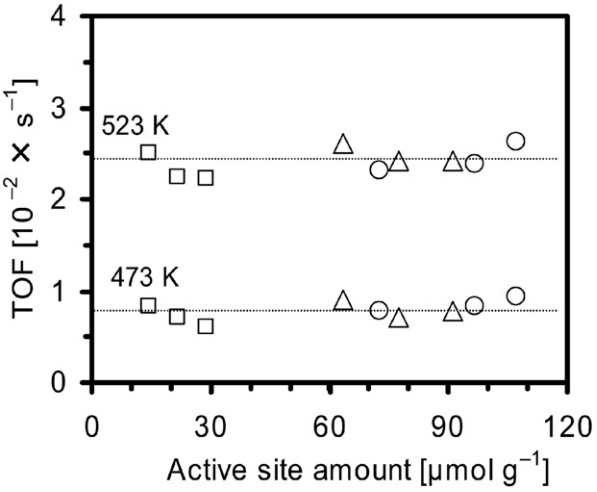

Fig. 14. TOF for NH_3-SCR as a function of the active site amount over (×) H-ZSM-5 and Fe/ZSM-5 prepared by (□) Imp, (△) RSIE, and (○) CVD. The active site amount is calculated by subtracting the NO_x desorption amount of H-ZSM-5 from that of Fe/ZSM-5.

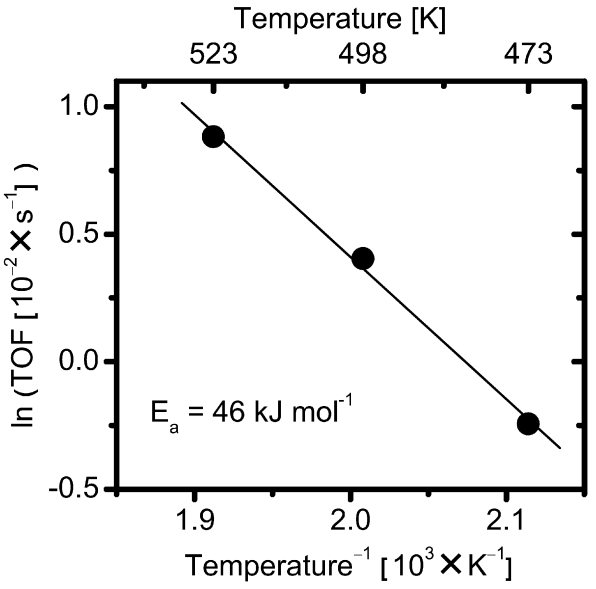

Fig. 15. Arrhenius plot of the logarithm of TOF versus inverse temperature (523–473 K).

Acknowledgments

The authors acknowledge Mr. Yuzo Kawai (TOYOTA Central R&D Labs.) for the ICP analysis and Mr. Hiroshi Nishioji (TORAY Research Center) for Mössbauer measurements.

References

[1] R.Q. Long, R.T. Yang, J. Am. Chem. Soc. 121 (1999) 5595.
[2] A.-Z. Ma, W. Grünert, Chem. Commun. (1999) 71.
[3] M.S. Kumar, M. Schwidder, W. Grünert, A. Brückner, J. Catal. 227 (2004) 384.
[4] M. Schwidder, M.S. Kumar, K. Klementiev, M.M. Pohl, A. Brückner, W. Grünert, J. Catal. 231 (2005) 314.
[5] K. Krishna, G.B.F. Seijer, C.M. van den Bleek, M. Makkee, G. Mul, H.P.A. Calis, Catal. Lett. 86 (2003) 121.
[6] G. Delahay, D. Valade, A. Guzmán-Vargas, B. Coq, Appl. Catal. B 55 (2005) 149.
[7] R. Joyner, M. Stockenhuber, J. Phys. Chem. B 103 (1999) 5963.
[8] H.-Y. Chen, W.M.H. Sachtler, Catal. Today 42 (1998) 73.
[9] F. Heinrich, C. Schmidt, E. Löffler, M. Menzel, W. Grünert, J. Catal. 212 (2002) 157.

[10] A.A. Battiston, J.H. Bitter, D.C. Koningsberger, J. Catal. 218 (2003) 163.
[11] A. Guzmán-Vargas, G. Delahay, B. Coq, E. Lima, P. Bosch, J.-C. Jumas, Catal. Today 107–108 (2005) 94.
[12] K.A. Dubkov, N.S. Ovanesyan, A.A. Shteinman, E.V. Starokon, G.I. Panov, J. Catal. 207 (2002) 341.
[13] El-M. El-Malki, R.A. van Santen, W.M.H. Sachtler, J. Catal. 196 (2000) 212.
[14] K. Krishna, M. Makkee, Catal. Lett. 106 (2006) 183.
[15] P.K. Roy, G.D. Pirngruber, J. Catal. 227 (2004) 164.
[16] A. Ribera, I.W.C.E. Arends, S. de Vries, J. Pérez-Ramírez, R.A. Sheldon, J. Catal. 195 (2000) 287.
[17] R.Q. Long, R.T. Yang, J. Catal. 201 (2001) 145.
[18] A.A. Battiston, J.H. Bitter, F.M.F. de Groot, A.R. Overweg, O. Stephan, J.A. van Bokhoven, P.J. Kooyman, C. van der Spek, G. Vankó, D.C. Koningsberger, J. Catal. 213 (2003) 251.
[19] E.J.M. Hensen, Q. Zhu, M.M.R.M. Hendrix, A.R. Overweg, P.J. Kooyman, M.V. Sychev, R.A. van Santen, J. Catal. 221 (2004) 560.
[20] P. Marturano, L. Drozdová, A. Kogelbauer, R. Prins, J. Catal. 192 (2000) 236.
[21] T. Nobukawa, M. Yoshida, K. Okumura, K. Tomishige, K. Kunimori, J. Catal. 229 (2005) 374.
[22] Q. Sun, Z.-X. Gao, H.-Y. Chen, W.M.H. Sachtler, J. Catal. 201 (2001) 89.
[23] G.D. Pirngruber, P.K. Roy, R. Prins, Phys. Chem. Chem. Phys. 8 (2006) 3939.
[24] L. Čapek, V. Kreibich, J. Dědeček, T. Grygar, B. Wichterlová, Z. Sobalík, J.A. Martens, R. Brosius, V. Tokarová, Microporous Mesoporous Mater. 80 (2005) 279.
[25] J. Torrent, V. Barrón, Clays Clay Miner. 51 (2003) 309.
[26] L. Lu, L. Li, X. Wang, G. Li, J. Phys. Chem. B 109 (2005) 17151.
[27] L.J. Lobree, I.-C. Hwang, J.A. Reimer, A.T. Bell, J. Catal. 186 (1999) 242.
[28] R.Q. Long, R.T. Yang, J. Catal. 194 (2000) 80.
[29] R.Q. Long, R.T. Yang, Catal. Lett. 74 (2001) 201.
[30] J. Jia, B. Wen, W.M.H. Sachtler, J. Catal. 210 (2002) 453.
[31] G.D. Pringruber, P.K. Roy, N. Weiher, J. Phys. Chem. B 108 (2004) 13746.
[32] C. Schmidt, T. Sowade, E. Löffler, A. Birkner, W. Grünert, J. Phys. Chem. B 106 (2002) 4085.
[33] B.S. Kwak, W.M.H. Sachtler, J. Catal. 141 (1993) 729.
[34] M.M. Mohamed, T.M. Salama, A.I. Othman, G.A. El-Shobaky, Appl. Catal. A 279 (2005) 23.
[35] H.H. Tippins, Phys. Rev. B 1 (1970) 126.
[36] W. Kündig, H. Bömmel, Phys. Rev. 142 (1966) 327.
[37] R.Q. Long, R.T. Yang, J. Catal. 198 (2001) 20.
[38] K. Sugawara, T. Nobukawa, M. Yoshida, Y. Sato, K. Okumura, K. Tomishige, K. Kunimori, Appl. Catal. B 69 (2007) 154.
[39] T. Nobukawa, K. Sugawara, K. Okumura, K. Tomishige, K. Kunimori, Appl. Catal. B 70 (2007) 342.
[40] T. Nobukawa, M. Yoshida, S. Kameoka, S. Ito, K. Tomishige, K. Kunimori, J. Phys. Chem. B 108 (2004) 4071.
[41] Z.X. Gao, Q. Sun, W.M.H. Sachtler, Appl. Catal. B 33 (2001) 9.
[42] M. Mauvezin, G. Delahay, B. Coq, S. Kieger, J.C. Jumas, J.O. Fourcade, J. Phys. Chem. B 105 (2001) 928.
[43] B. Wichtelová, Z. Sobalík, J. Dědeček, Appl. Catal. B 41 (2003) 97.
[44] J. Jia, Q. Sun, B. Wen, L.X. Chen, W.M.H. Sachtler, Catal. Lett. 82 (2002) 7.
[45] K. Lázár, A.N. Kotasthane, P. Fejes, Catal. Lett. 57 (1999) 171.
[46] J.A. Rodriguez, T. Jirsak, S. Sambasivan, D. Fischer, A. Maiti, J. Chem. Phys. 112 (2000) 9929.
[47] A. Vimont, F.T. Starzyk, J.C. Lavalley, J. Phys. Chem. B 104 (2000) 286.
[48] M.S. Kumar, M. Schwidder, W. Grünert, U. Bentrup, A. Brückner, J. Catal. 239 (2006) 173.
[49] A.R. Overweg, M.W.J. Crajé, A.M. van der Kraan, I.W.C.E. Arends, A. Ribera, R.A. Sheldon, J. Catal. 223 (2004) 262.
[50] W.M. Heijboer, P. Glatzel, K.R. Sawant, R.F. Lobo, U. Bergmann, R.A. Barrea, D.C. Koningsberger, B.M. Weckhuysen, F.M.F. de Groot, J. Phys. Chem. B 108 (2004) 10002.
[51] M. Devadas, O. Kröcher, A. Wokaun, React. Kinet. Catal. Lett. 86 (2005) 347.